Geomechanics and Engineering, *Vol. 24, No. 1 (2021) 67-79*
DOI: https://doi.org/10.12989/gae.2021.24.1.067

Seismic response of utility tunnels subjected to different earthquake excitations

Chenglong Wang[1,2], Xuanming Ding[1,2], Zhixiong Chen*[1,2], Li Feng[1,2] and Liang Han[1,2]

[1]*College of Civil Engineering, Chongqing University, Chongqing, 400045, China*
[2]*Key Laboratory of New Technology for Construction of Cities in Mountain Area, Ministry of Education, Chongqing, 400045, China*

(Received January 18, 2020, Revised December 22, 2020, Accepted December 28, 2020)

Abstract. The influence of ground motions on the seismic response of utility tunnels was investigated. A series of small-scale shaking table model tests were carried out under uniform excitation in the transverse direction. Different peak accelerations of EL-Centro and Taft earthquake waves were applied. The acceleration responses, earth pressure, seismic strain, bending moment and structure deformations were measured and discussed. The results showed that the types of earthquake waves had significant influences on the soil-structure acceleration responses. However, the amplitude of the soil acceleration along the depth showed consistent variation regardless of the types of earthquake waves and tunnels. The horizontal soil pressure near the top and bottom slabs showed obviously larger values than those at other depths. In general, the strain response in the outer surface was more significant than that on the inner surface, and the peak strain in the end section of the model was larger than that in the middle section. Moreover, the bending moment at the corner points was much larger than that at middle point, and the bending moment was greatly affected by both input accelerations and seismic wave types. The opposite direction of shear deformation on the top and bottom slabs presented a rotation trend of the model structure.

Keywords: utility tunnels; seismic response; shaking table tests; earthquake waves; transverse excitation

1. Introduction

Utility tunnels are becoming a more important part of underground structures, because they are involved in a wide range of applications, including water supply, sewage treatment, natural gas and oil supply, telecommunication facilities and underground maintenance (Chen *et al*. 2012). Much attention has been given to the seismic safety of utility tunnels, as recent earthquake observations (1995 Kobe earthquake, 1999 Duzce earthquake, 1999 Chi-chi earthquake, 2003 Bam earthquake, 2008 Wenchuan earthquake) have indicated that underground structures may experience severe damage or collapse due to seismic loading (Cilingir 2011, Yu *et al*. 2013, Wang *et al*. 2015). Furthermore, the seismic performance of embedded structures is different from that of above-ground structures. The kinematic load provided by the surrounding soil is larger than the inertial loads induced by the oscillation of the structure itself (Tsinidis *et al*. 2015).

To investigate the dynamic behavior of underground structures, many researchers have conducted a series of studies (Chou *et al*. 2010, Debiasi *et al*. 2013, Liu *et al*. 2014, Baziar *et al*. 2014, Yan *et al*. 2015, Xu *et al*. 2016, Chen *et al*. 2017, Wang *et al*. 2017, Kwak *et al*. 2018, Yan *et al*. 2018, Liu *et al*. 2018, Fan *et al*. 2019, Zhang *et al*. 2019, Sun *et al*. 2019, Ding *et al*. 2020). Abuhajar *et al*. (2015a, b) and Tsinidis *et al*. (2016, 2017) conducted a combined centrifuge model and numerical study on the seismic response of box-type tunnels. Yu *et al*. (2018a, 2019) proposed analytical solutions for the seismic activity of tunnel lines considering longitudinal bending stiffness and sharp stiffness transition. Yu *et al*. (2018b, c) and Yuan *et al*. (2018) conducted a series of shaking table tests to investigate the seismic performance of a long tunnel under non-uniform earthquake excitation. However, these studies mainly focused on the seismic performance of traffic tunnels, and utility tunnels typically have smaller cross sections than traffic tunnels. Moreover, utility tunnels are cut-and-cover structures that have higher seismic vulnerability than circular bored tunnels (Hashash *et al*. 2001).

Due to a lack of reliable analytical or empirical tools, model tests are increasingly being adopted to study the seismic response of utility tunnels. In particular, large-scale shaking table tests are an efficient way to reproduce seismic excitation. Jiang *et al*. (2010) conducted shaking table tests to analyze the seismic performance of a utility tunnel model. They used the El-Centro earthquake wave as an input and found that the soil acceleration was slightly larger than the structural acceleration. They also noted that the internal force and earth pressure increased with increasing peak ground acceleration, which was verified with the established finite element model. Furthermore, they reported that the distribution of earth pressure on the top or bottom slab was different from that on the sidewalls. Chen *et al*. (2010) carried out a series of shaking table tests of a utility tunnel through two isolated shaking tables, and they comparatively analyzed the performance of a utility tunnel under uniform and non-uniform earthquake excitations.

*Corresponding author, Associate Professor
E-mail: chenzhixiong@cqu.edu.cn

ISSN: 2005-307X (Print), 2092-6219 (Online)

Their results showed that the structural response under non-uniform excitation was much larger than that under uniform excitation. They also noted that the effect of the spatial distribution of earthquake excitations should be evaluated. Chen *et al*. (2012) performed further numerical simulations of shaking table tests on utility tunnels under non-uniform earthquake excitation. Their numerical results had good agreement with the experimental values. Furthermore, the tunnel model exhibited bending deformation. Their results also showed that the acceleration response of the tunnel model was more obvious than that of the surrounding soil for high shaking intensity, which was different than the results reported by Jiang *et al*. (2010). Thus, the acceleration response needs to be further investigated.

Despite previous studies, there are still unanswered questions regarding the seismic response of utility tunnels under different input earthquake waves. Several issues including acceleration responses of soil and utility tunnels, distribution of soil-structure earth pressure, seismic strain of the structure, seismic bending moment on the slabs and sidewalls and complex deformation modes of utility tunnels, are still not well understood. This paper explores the above issues by means of a shaking table test under uniform excitation in the transverse direction. EL-Centro and Taft earthquake waves with different peak accelerations were input to comparatively analyze the dynamic behavior of the soil-structure.

2. Experimental methods

2.1 Shaking table system

The model test was performed on a shaking table with dimensions of 1.2 m × 1.2 m (length × width). The designed maximum load of the shaking table was 10 kN, and the operating frequency ranged from 0~50 Hz. The maximum acceleration of the shaking table was 1.2 g with a full load of 10 kN, and 2.0 g with a load less than 5 kN in the horizontal and vertical directions, respectively. The maximum displacement of 100 mm and the maximum velocity of 0.5 m/s were observed in each direction.

A laminar shear box composed of 12 steel frames was utilized as the soil container as shown in Fig. 1(a), which had dimensions of 650 mm × 850 mm × 950 mm (height × width × length). The frame could move freely in two horizontal directions (longitudinal and transverse). Fig. 1(b) shows the placement of the model structure in the soil container.

2.2 Model structure

In the shaking table test, the geometrical scale was defined as 1:15 in consideration of the capacity of the shaking table and soil container. The geometric length (L), stress (σ) and acceleration (a) were characterized as the basic physical variables. Table 1 shows the similitude relations and ratios according to the Buckingham π theorem. The utility tunnel model had a rectangular cross-section. According to Table 1, the utility tunnel model was 800 mm long (L), 233 mm wide (D), 300 mm high (H), and

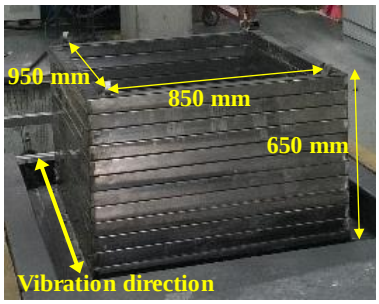

(a) Laminar shear box

(b) Model structure

Fig. 1 Shaking table system

Table 1 Model test scale factors

Physical quantities	Peak acceleration	Similitude ratio
Length	S_L	1/15
Stress	S_σ	1/3
Elastic module	$S_\sigma = S_E$	1/3
Acceleration	S_a	5.0
Density	$S_\rho = S_E/(S_a S_L)$	1.0
Frequency	$S_f = \sqrt{S_a/S_L}$	8.66
Time	$S_t = S_f^{-1}$	0.1154

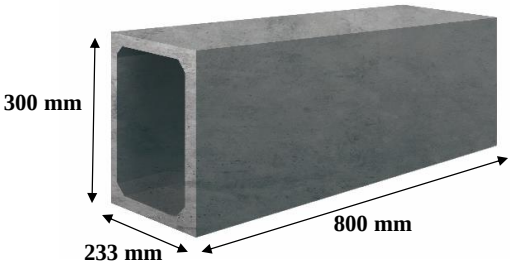

Fig. 2 Utility tunnel model

20 mm thick (T). The detailed dimensions of the model are shown in Fig. 2. Micro-concrete and wire with a diameter of 2.8 mm were used to simulate normal concrete and rebar, respectively.

Fig. 3 shows the layout of the model tunnel. In the transverse direction, the utility tunnel model was located nearly 358 mm away from two soil boundaries. In the longitudinal direction, a space of 25 mm was reserved between the soil boundary and the two ends of the utility tunnel, and this space was filled with polystyrene foam board to prevent the soil from flowing into the tunnel. In the vertical direction, the distance from the soil boundary to the

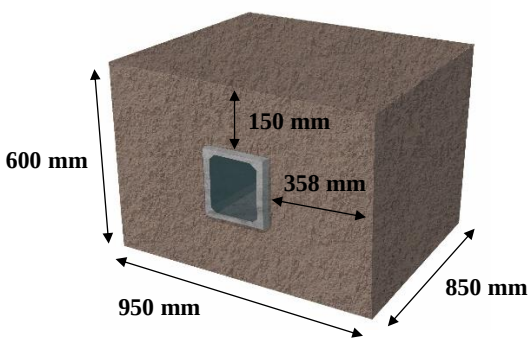

Fig. 3 Layout of the model tunnel

Table 2 Soil characteristics

Material	D_{10}(mm)	D_{30}(mm)	D_{50}(mm)	D_{60}(mm)	G_s	C_u	C_c
Sand	0.16	0.37	0.60	0.72	2.63	4.50	1.19

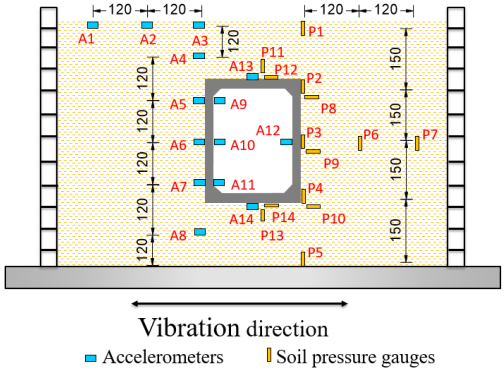

(a) Layout of sensors

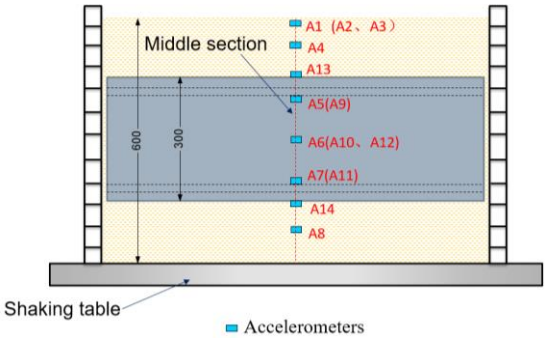

(b) Side view

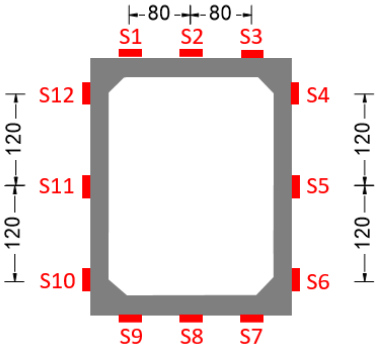

(c) End section

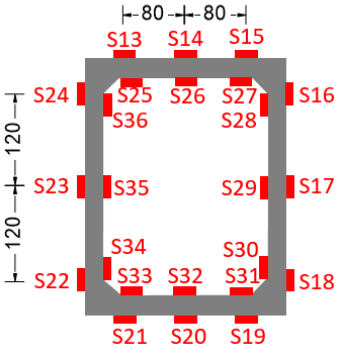

(d) Middle section

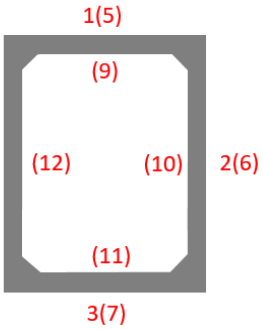

(e) Labelled surface

Fig. 4 Schematic diagram of the model test (unit: mm)

structure surface was 150 mm.

2.3 Soil properties

Fujian sand was used in the model test. The maximum and minimum dry densities of the sand were 1.64 and 1.35 g/cm³, respectively. The sand characteristics are shown in Table 2. In addition, the dynamic characteristics of Fujian standard sand were reported by Li *et al*. (2017). The soil layer was compacted every 100 mm, and the relative density reached 75-80%.

2.4 Instruments of the tests

Fig. 4 shows the layout of the instruments. The letters A, P, and S indicate the accelerometer, earth pressure cell, and strain gauge, respectively. In this test, 14 accelerometers were installed to measure the horizontal acceleration response of the structure and soil. As shown in Fig. 4(a), earth pressure cells P1, P2, P3, P4, P5, P6, P7, P11, and P13 were used to measure the horizontal soil pressure. P8, P9, P10, P12, and P14 were used to measure the vertical soil pressure. Fig. 4(b) shows the side view of the test model.

Table 3 Test cases

Case	Excitation waves	Peak of inputted ground acceleration	Vibration direction
1	EL-Centro	0.2 g	transversal
2	EL-Centro	0.4 g	transversal
3	EL-Centro	0.8 g	transversal
4	EL-Centro	1.2 g	transversal
5	Taft	0.2 g	transversal
6	Taft	0.4 g	transversal
7	Taft	0.8 g	transversal
8	Taft	1.2 g	transversal

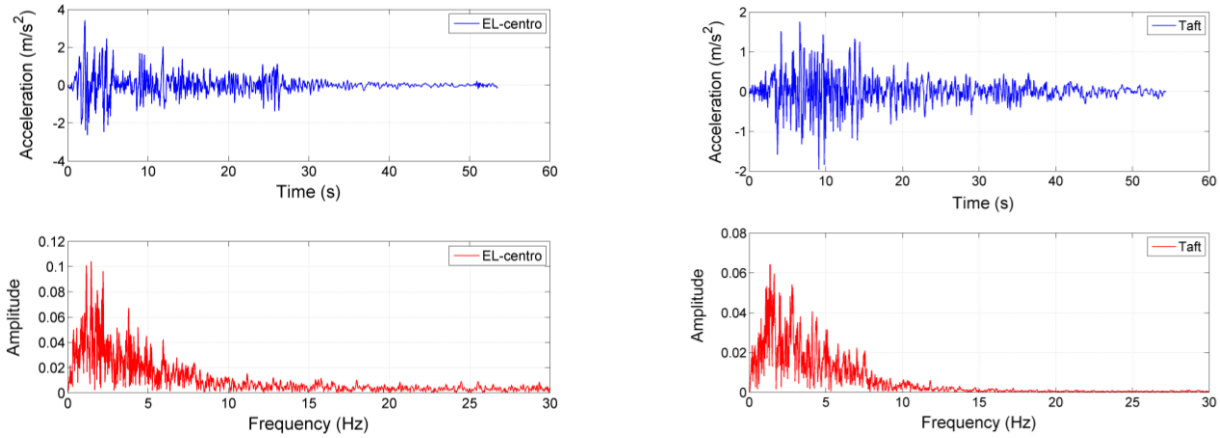

(a) EL-Centro (b) Taft

Fig. 5 Acceleration time histories and Fourier spectra of input motions

2.5 Input earthquake motions

The test cases are shown in Table 3. The prototype earthquake waves EL-Centro and Taft were selected as the input earthquake motions representatively. Figs. 5(a) and 5(b) show the time history and auto-spectra of the EL-Centro and Taft waves. The utility tunnel is a shallow-buried slender structure, which is more vulnerable under transverse vibration (perpendicular to the utility tunnel axis). Therefore, this test adopted transverse vibration under uniform earthquake excitation. According to the similitude ratio shown in Table 1, the duration of the earthquake wave decreased to 0.115 times that of the seismic records. The peak ground acceleration (PGA) of the two waves was designed at 0.2 g, 0.4 g, 0.8 g, and 1.2 g for comparative analysis.

3. Experimental results

3.1 Verification of boundary effect

The boundary effect of the soil container is unavoidable in shaking table tests. It is essential to explore this problem in the model test. In this test, the soil peak accelerations at A1 and A2 are normalized by that at A3 to evaluate the boundary effect. Fig. 6 shows the acceleration ratios at different input acceleration amplitudes. The ratios of A1/A3 and A2/A3 for the two waves ranged from 0.82 to 1.15, which were close to 1, implying that the acceleration responses were similar at these points (Yan *et al*. 2018).

Figs. 7(a) and 7(b) show the acceleration spectra at 0.2 g for the EL-Centro and Taft wave cases, respectively. The Fourier spectra at A1, A2, and A3 exhibited the same variation trend. Furthermore, the predominant frequency and corresponding amplitude measured at those points exhibited negligible differences. Thus, the results in Fig. 6 and Fig. 7 show that the boundary effect was insubstantial in this test.

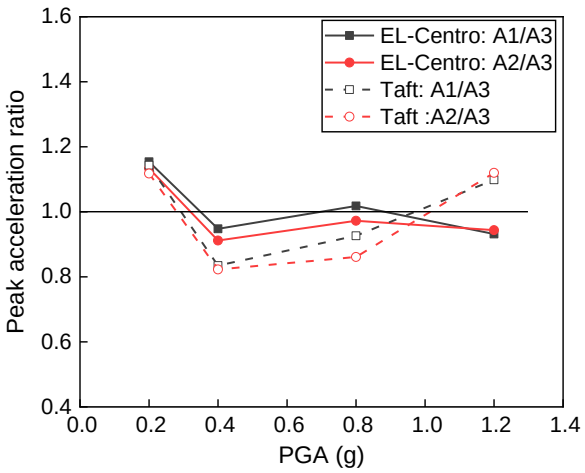

Fig. 6 Acceleration ratios at different PGAs

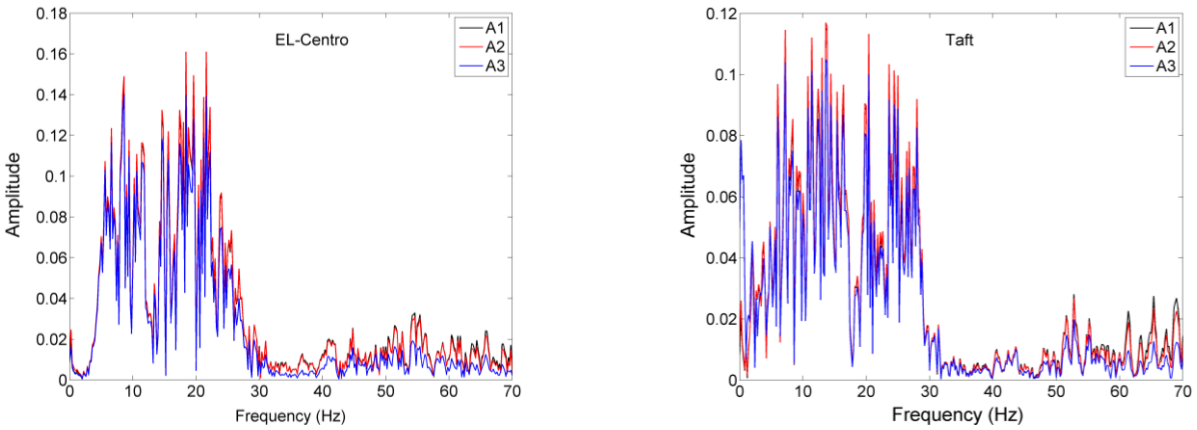

(a) EL-Centro (b) Taft

Fig. 7 Acceleration spectra of soil surface at 0.2 g

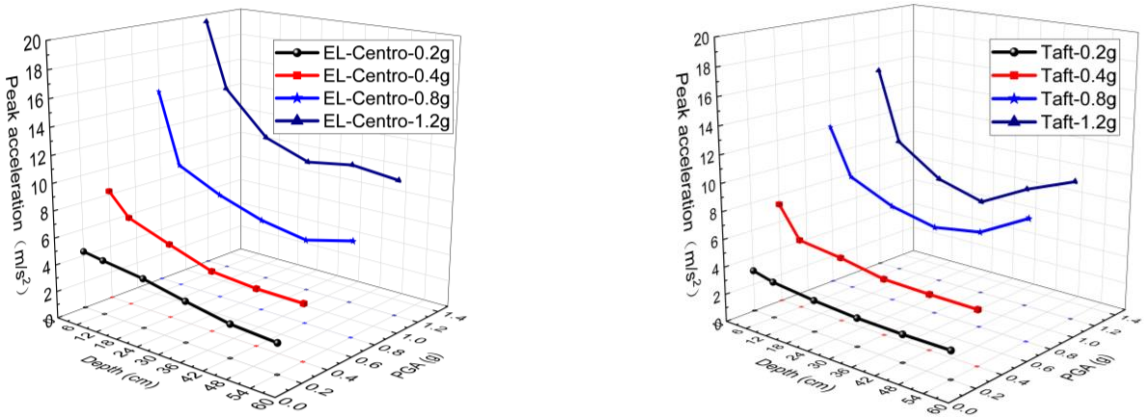

(a) EL-Centro (b) Taft

Fig. 8 Peak acceleration values for different PGAs

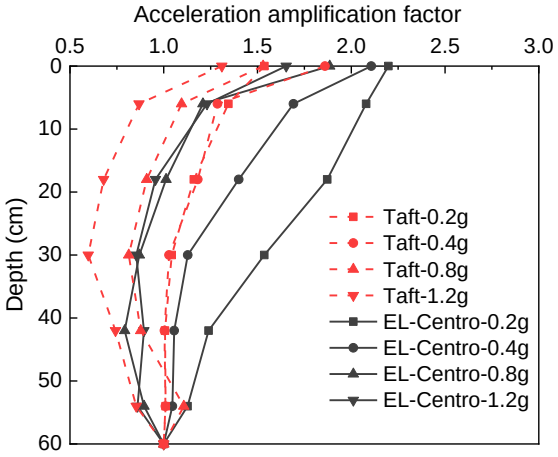

Fig. 9 Variation in the soil acceleration amplification factor along the depth

3.2 Acceleration response

Fig. 8 shows the peak acceleration values for different PGAs. The peak acceleration decreased with increasing depth at a small PGA. However, as the PGA increased to 0.8g, the peak acceleration first decreased and then decreased with increasing depth, indicating an obvious development of soil nonlinearity. In addition, the curve trends of the seismic waves of EL-Centro and Taft were similar.

Fig. 9 shows the distribution of the acceleration amplification factor, which is defined as the ratio of the measured peak acceleration to the input peak acceleration (IPA) (Chen *et al*. 2017). In general, the soil acceleration amplification factor at each point decreased with increases in PGA. Consequently, an acceleration amplification factor less than 1 was observed at PGA=0.8 g and 1.2 g. It could also be found that the amplification factor decreased with increasing depth for PGA≤0.4 g, whereas the amplification factor tended to first increase and then decrease with increasing depth for PGA≥0.8 g. This phenomenon was due to the development of soil nonlinearity, resulting in large soil deformation at a high PGA, which was similar to the results reported by Chen *et al*. (2010) under non-uniform earthquake excitation. Furthermore, the development of soil nonlinearity for the utility tunnel was similar to that for a square traffic tunnel (Tsinidis *et al*. 2016), an immersed tunnel (Chen *et al*. 2017) and a deep buried line (Yan *et al*. 2018). This figure also indicated that the amplification factor under the Taft wave was generally smaller than that under the EL-Centro wave at the same PGA, except for a few measured points.

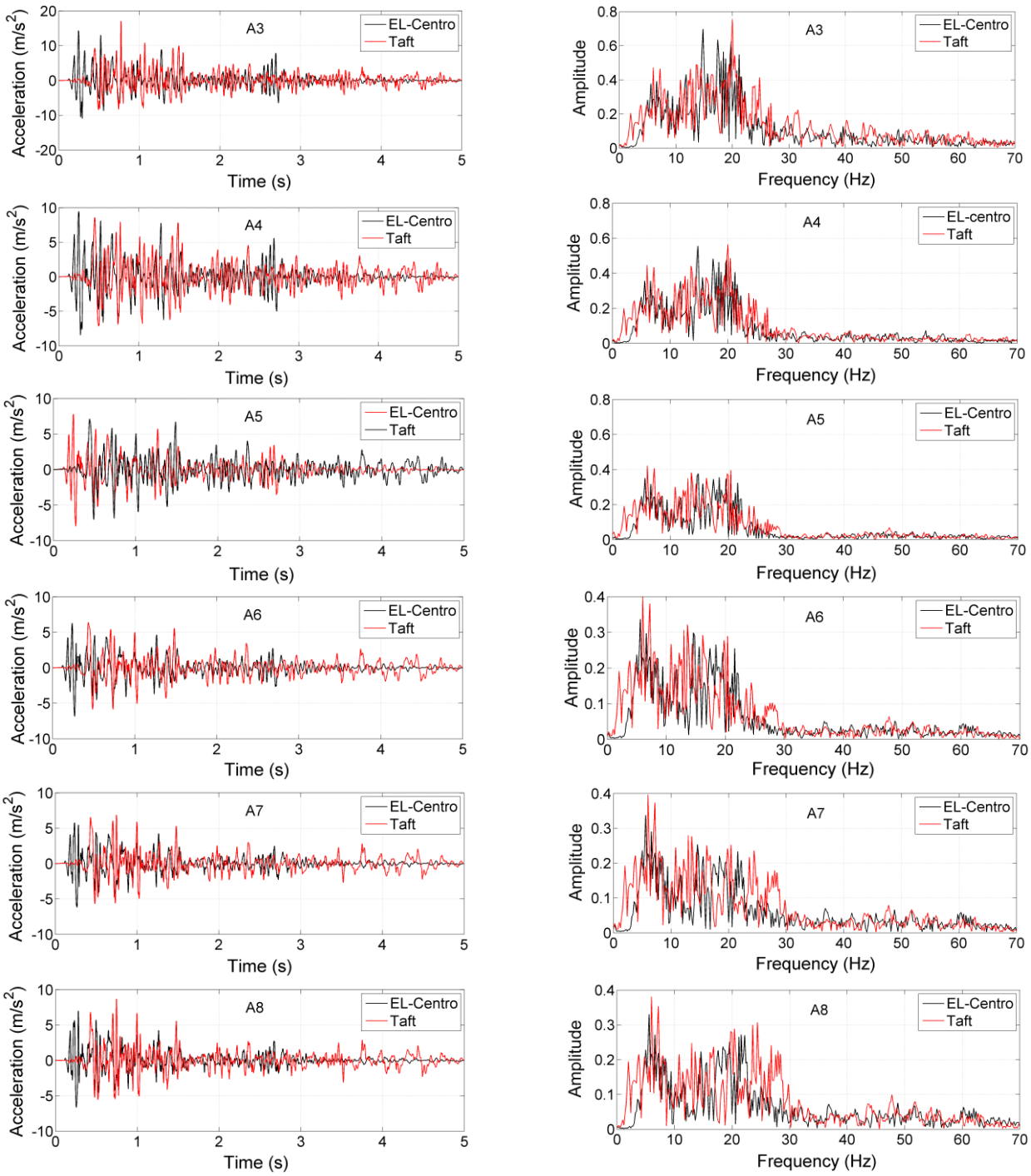

Fig. 10 Acceleration time histories and corresponding Fourier spectra in the vertical direction (PGA=0.8 g)

Fig. 10 shows the acceleration time histories and corresponding Fourier spectra of the soil at different depths for PGA =0.8 g. The amplitude of acceleration first decreased (A4, A5, and A6) and then increased obviously (A6, A7, and A8) from the soil surface to the bottom, which was the same as the trend of the amplification factor. Under the EL-Centro wave, the predominant frequencies measured by A6, A7, and A8 were all 5.6 Hz, whereas those measured by A3, A4, and A5 were 14.8 Hz. Under the Taft wave, the predominant frequencies recorded by A5, A6, A7, and A8 were 6 Hz, whereas those recorded by A3 and A4 were 20 Hz. These findings occur because of the filtering effect on the low-frequency components and the amplification effect on the high-frequency components (Shi 2008).

Fig. 11 shows a comparison of peak accelerations between the structure and its surrounding soil. The sensors A9, A10, and A11 were placed on the inner surface of the left sidewall to monitor the accelerations of the structure. Under the EL-Centro wave at PGA≤0.8 g, the accelerations of the soil and structure decreased with increasing depth, showing the strongest shaking response in the upper part. At PGA=1.2 g, the largest acceleration of the structure was measured at the middle point, consistent with the surrounding soil. Moreover, the structural accelerations in

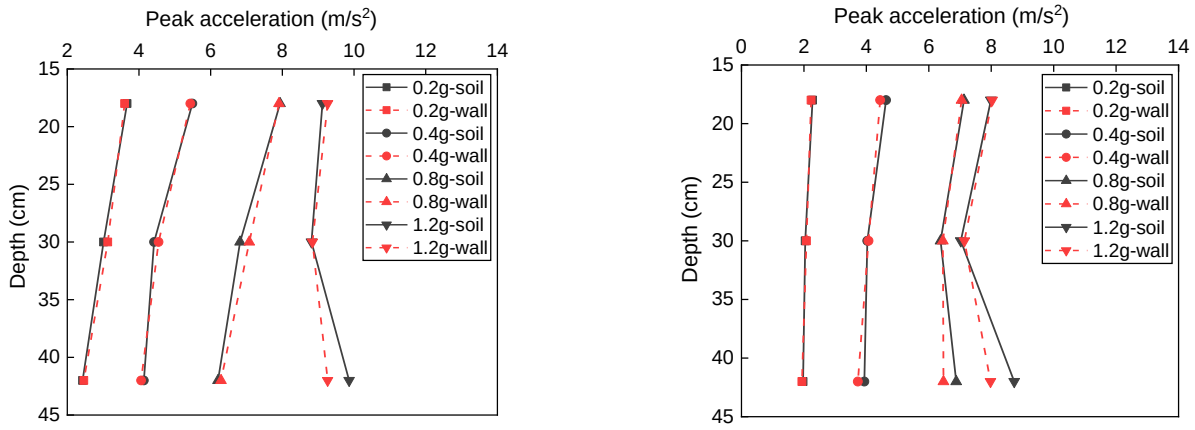

(a) Wind speed profile (b) Wind direction profile

Fig. 11 Comparison of peak accelerations between the sidewall and the surrounding soil along the depth

Table 4 Acceleration response of the two sidewalls under the EL-Centro wave

PGA (g)	Measured points	Peak acceleration (g)	Amplification factor	Predominant frequency (Hz)	Amplitude
0.2 g	A(10)	0.319	1.597	8.6	0.126
	A(12)	0.304	1.520	8.6	0.130
0.4 g	A(10)	0.464	1.160	8.6	0.199
	A(12)	0.457	1.144	8.6	0.199
0.8 g	A(10)	0.722	0.903	5.6	0.345
	A(12)	0.709	0.887	5.6	0.347
1.2 g	A(10)	0.026	0.022	0.2	0.091
	A(12)	0.038	0.031	0.2	0.132

Table 5 Acceleration response of the two side walls under the Taft wave

PGA (g)	Measured points	Peak acceleration (g)	Amplification factor	Predominant frequency (Hz)	Amplitude
0.2 g	A(10)	0.212	1.061	7.2	0.103
	A(12)	0.216	1.078	7.2	0.105
0.4 g	A(10)	0.415	1.038	7.2	0.212
	A(12)	0.406	1.016	7.2	0.215
0.8 g	A(10)	0.658	0.823	6.0	0.412
	A(12)	0.665	0.831	6.0	0.412
1.2 g	A(10)	0.728	0.607	6.0	0.469
	A(12)	0.723	0.602	6.0	0.468

the middle depth were larger than those in the surrounding soil, which is similar to the results reported by Chen *et al.* (2012). However, the overall acceleration difference between the sidewall and the surrounding soil was small. In Fig. 11(b), the distribution of accelerations under the Taft wave was similar to that under the EL-Centro wave except when PGA=0.8 g. This indicated that the separation of soil and the structure possibly occurred near the lower ends of the structure as PGA increased.

To investigate the acceleration response of the two sidewalls, the accelerations recorded by A10 and A12 were analyzed in Tables 4 and 5. In terms of frequency characteristics, the predominant frequency was consistent on both sidewalls of the structure, and the corresponding amplitudes were approximately the same except for a slight difference at PGA=1.2 g under the EL-Centro wave. As the PGA increased, the predominant frequency tended to decrease, whereas the corresponding amplitude exhibited an increasing trend. In addition, the peak values of acceleration measured by A10 and A12 were basically the same, and the corresponding amplification factors had negligible differences. This finding indicates that the seismic acceleration responses of the two sidewalls are consistent.

The accelerations recorded by A13 and A14 were comparatively analyzed to investigate the acceleration response on the top and bottom slabs. The results are shown in Tables 6 and 7. In terms of the frequency response, the predominant frequency at the top of the structure was

Table 6 Acceleration response of the top and bottom slabs under the EL-Centro wave

PGA (g)	Measured points	Peak acceleration (g)	Amplification factor	Predominant frequency (Hz)	Amplitude
0.2 g	A(13)	0.404	2.018	8.6	0.134
	A(14)	0.240	1.202	8.6	0.114
0.4 g	A(13)	0.702	1.756	18.4	0.272
	A(14)	0.440	1.100	5.6	0.185
0.8 g	A(13)	0.945	1.186	14.8	0.459
	A(14)	0.672	0.840	5.6	0.328
1.2 g	A(13)	0.023	0.019	0.2	0.078
	A(14)	0.007	0.006	0.2	0.014

Table 7 Acceleration response of the top and bottom slabs under the Taft wave

PGA (g)	Measured points	Peak acceleration (g)	Amplification factor	Predominant frequency (Hz)	Amplitude
0.2 g	A(13)	0.248	1.239	7.2	0.108
	A(14)	0.211	1.053	7.2	0.098
0.4 g	A(13)	0.513	1.282	20.4	0.261
	A(14)	0.423	1.057	7.2	0.198
0.8 g	A(13)	0.904	1.130	20	0.495
	A(14)	0.838	1.047	6.0	0.382
1.2 g	A(13)	0.986	0.822	20.4	0.570
	A(14)	1.048	0.873	6.0	0.433

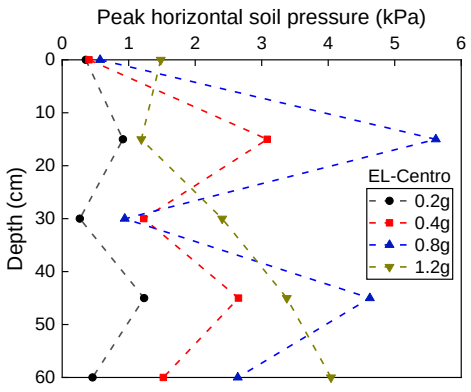

(a) EL-Centro

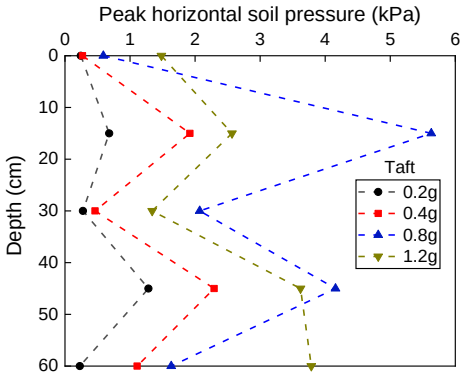

(b) Taft

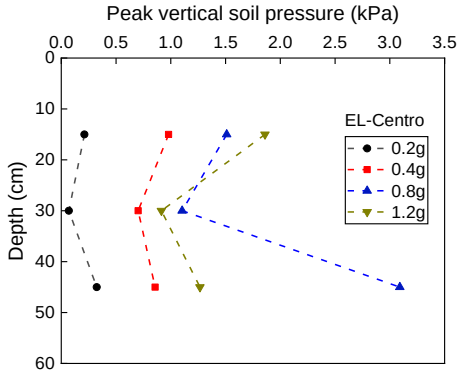

(c) EL-Centro

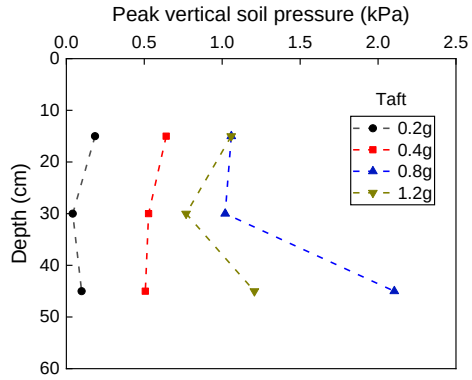

(d) Taft

Fig. 12 Seismic response of soil pressure

generally larger than that at the bottom, and the corresponding amplitude also had a slight difference. The peak acceleration at the top slab was larger than that at the bottom slab. Under the EL-Centro wave, the differences reached 67.8%, 71.2% and 41.2% for PGA = 0.2 g, 0.4 g and 0.8 g, respectively. Under the Taft wave, the differences reached only 17.7%, 21.3%, and 58.0% for PGA = 0.2 g, 0.4 g and 0.8 g, respectively. Due to the difference in the peak acceleration response, the amplification factor at the top of the structure was larger than that at the bottom. In addition, the amplification factor usually decreased with increasing PGA under different wave types.

3.3 Soil and structure earth pressure

Figs. 12(a) and 12(b) shows the peak horizontal soil pressure along the depth under different PGAs, as measured by P1, P2, P3, P4 and P5. The distribution curves of horizontal soil pressure under the EL-Centro and Taft waves were similar for PGA≤0.8 g, wherein the curves were roughly "W" shaped. Along the right sidewall, the horizontal soil pressure was larger at the upper and lower points and much smaller in the middle part. This discrepancy existed due to the influence of the sidewall restraint on the movement of the surrounding soil during the vibration process, especially near the structural corners.

The horizontal soil pressure increased generally as PGA increased to 0.8 g, whereas, it would decrease obviously for PGA=1.2 g. This phenomenon was probably due to the development of soil nonlinearity, resulting in large soil deformation at a high PGA. Under the EL-Centro wave, the horizontal soil pressure near the upper and lower slabs of the structure was 180%~500% larger than that in the middle part for PGA≤0.8 g. However, for PGA=1.2 g, the smallest horizontal earth pressure was measured at the upper slab. This trend occurred probably because an overall slight tilt of the structure occurred, and the separation of soil and the structure was possibly produced near the upper ends of the structure as PGA increased, which reduced the horizontal dynamic soil pressure near the upper part of the structure. Furthermore, the peak horizontal soil pressure near the soil surface (P1) and bottom boundary (P5) was generally smaller than that at the sidewall, indicating that the horizontal soil pressure response was more obvious near the utility tunnel.

During the vibration process, although vibration was applied in the horizontal direction, the vibration still caused a response in the vertical soil pressure. Figs. 12(c) and 12(d) shows the peak vertical soil pressure along the structure surface. The distribution was similar to that of the horizontal soil pressure along the sidewall. The peak vertical soil pressures measured by P8, P9, and P10 had only a slight difference when PGA≤0.4 g, and the difference in these pressures increased when PGA≥0.8 g. Moreover, the seismic vertical soil pressure was generally smaller than the horizontal soil pressure in Fig. 12.

3.4 Strain analysis

In view of the previous earthquake cases, the underground structure will experience different degrees of cracking due to the large seismic internal strain was produced. As a result, the integrity and safety of the structure will be influenced. Moreover, the concrete permeability will change significantly, and the reinforcement will suffer severe corrosion. Thus, it is essential to investigate the response of seismic strain. To consider the most dangerous situation of the structure, the maximum strain is mainly analyzed here. In this shaking table test, transverse uniform seismic excitation was applied, inducing a vibration direction perpendicular to the axial direction of the utility tunnel. Therefore, transverse stress and strain were mainly generated in the vibration process of the structure. Fig. 13 shows the maximum positive (tensile) and negative (compressive) strain of the cross-section in the middle and end sections at PGA=0.8 g. This figure shows that the strain distributions under the EL-Centro and Taft waves were similar, and the strain values had only slight differences.

Figs. 13(a) and 13(b) show that the strain in the middle point was very small, whereas the strains were very large at the two symmetric corner points. In addition, the strains on surfaces 1 and 9 were similar, presenting good symmetry during the vibration process. In contrast, on surface 5, the strain in the right corner point was much larger than that in the left point. Figs. 13(c) and 13(d) show the strain response on the bottom slab, wherein the strain distributions were similar to those of the top slab. Nevertheless, the strain value on the bottom slab was much larger than that of the top slab, probably due to the larger bending moment of the bottom corner point. Figs. 13(a)-13(d) show that the strain on surface 5 was generally larger than that on surface 9, which indicated that the strain response on the outer surface was more obvious than that on the inner surface. In addition, the strain in the end section was larger than that in the middle section in most cases, especially for the bottom slab.

Figs. 13(e)-13(h) show the maximum strain responses of the two sidewalls in different sections. The strains near the two corners were much larger than those in the middle point. Moreover, on the left sidewall, the strain at the top corner was usually larger than that at the bottom corner. However, the result was opposite on the right sidewall. The outer surface strain response of the end section was more obvious than that of the middle section. Comparatively, the inner surface strain in the middle section was the smallest.

3.5 Seismic bending moment

To investigate the deformation behavior of the utility tunnel, the seismic bending moment is calculated based on the recorded test data. Due to the time history curve of the input seismic wave, the bending moment at different times also changes accordingly. Thus, to determine the maximum bending moment, the maximum seismic response and its corresponding moment generated from all the measuring points were explored. Then, the maximum bending moment was calculated according to the strain data at this time. The unit length (1 m) of the structure is taken to calculate the bending moment. The specific parameters are shown in Table 8, and the bending moment can be calculated as follows:

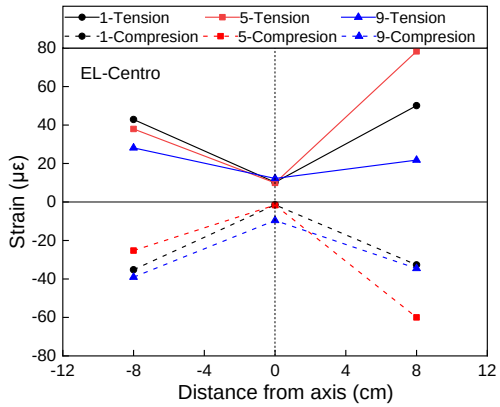

(a) Top slab (EL-Centro)

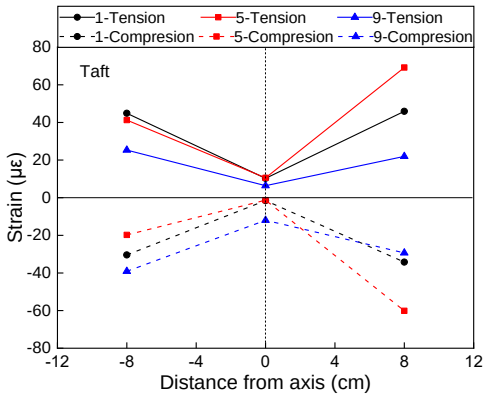

(b) Top slab (Taft)

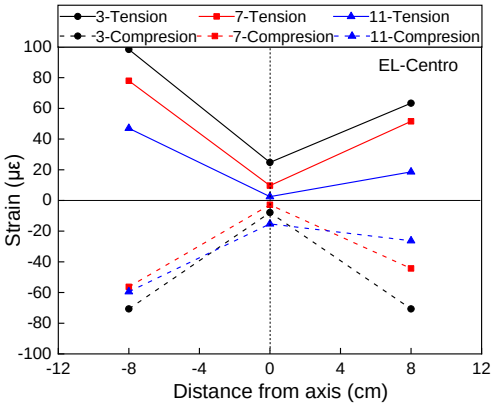

(c) Bottom slab (EL-Centro)

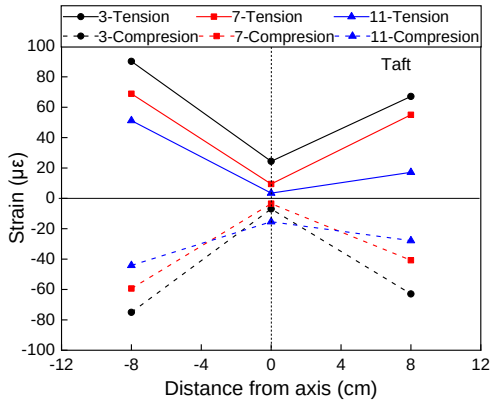

(d) Bottom slab (Taft)

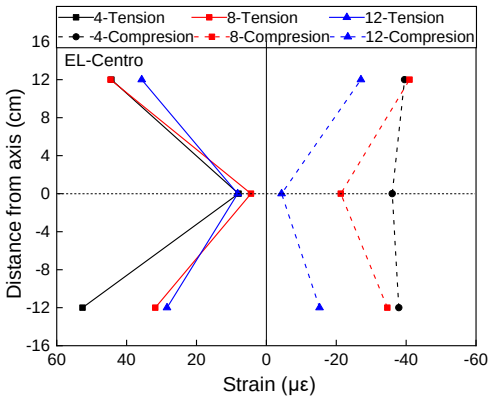

(e) Left side wall (EL-Centro)

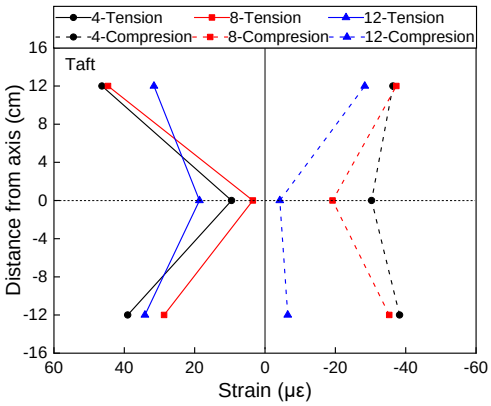

(f) Left side wall (Taft)

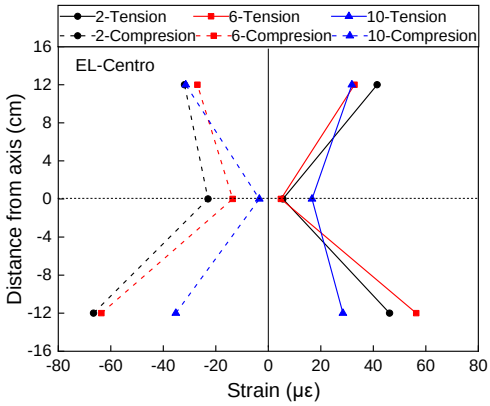

(g) Right side wall (EL-Centro)

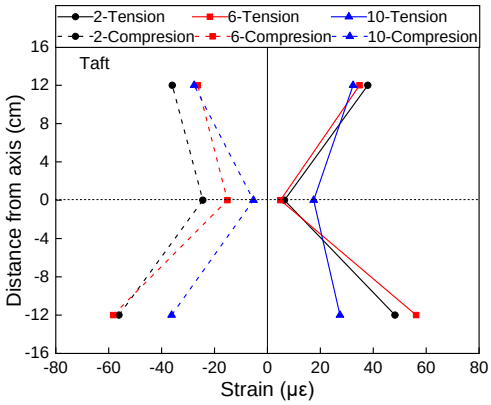

(h) Right side wall (Taft)

Fig. 13 Seismic response of strain (PGA=0.8 g)

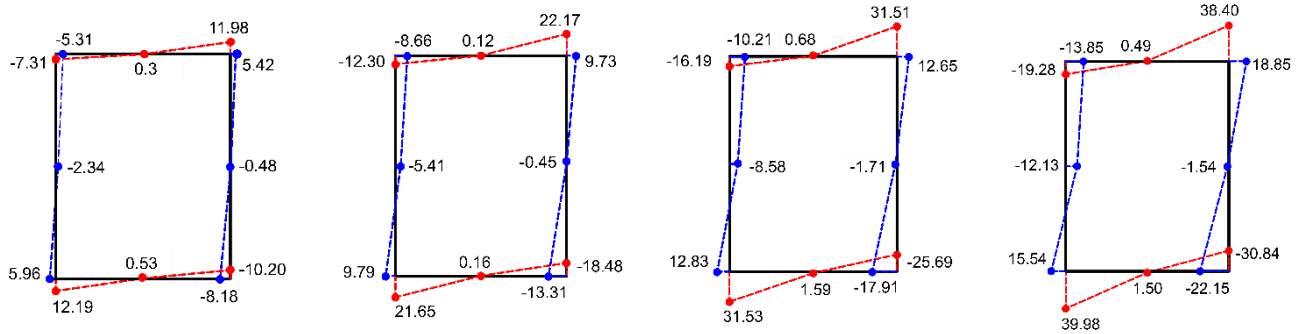

(a) 0.2 g (b) 0.4 g (c) 0.8 g (d) 1.2 g

EL-Centro wave (middle section)

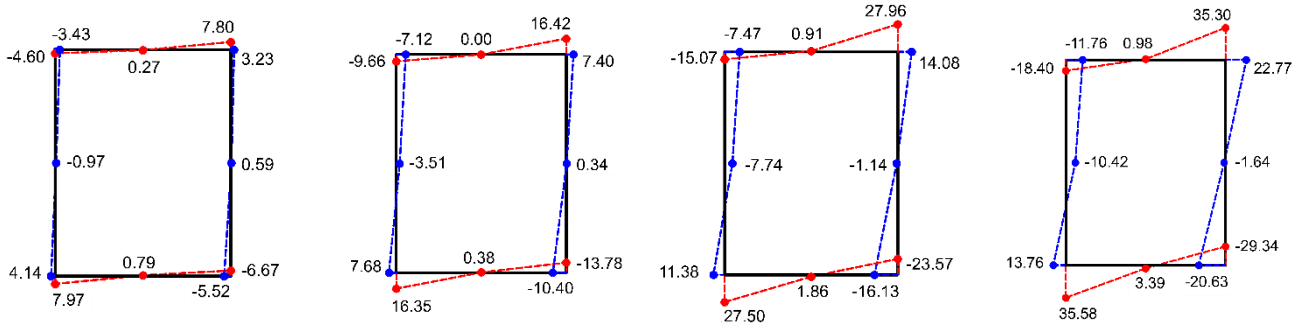

(e) 0.2 g (f) 0.4 g (g) 0.8 g (h) 1.2 g

Taft wave (middle section)

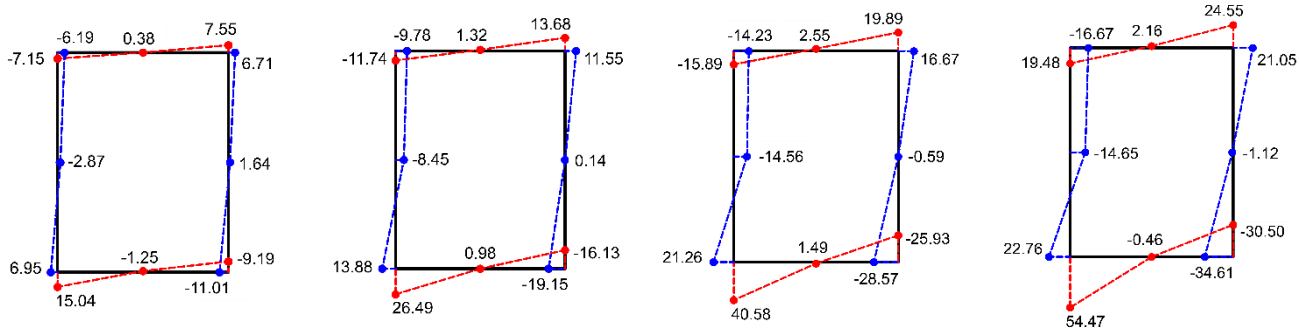

(i) 0.2 g (j) 0.4 g (k) 0.8 g (l) 1.2 g

EL-Centro wave (end section)

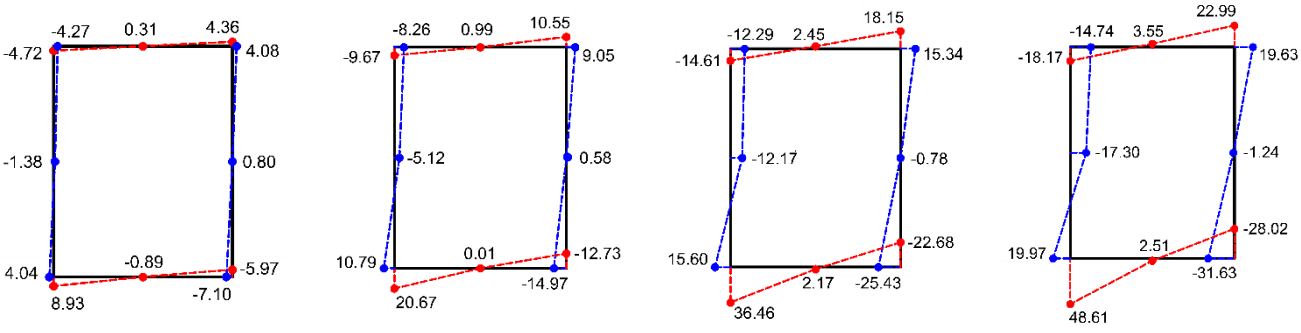

(m) 0.2 g (n) 0.4 g (o) 0.8 g (p) 1.2 g

Taft wave (end section)

Fig. 14 Seismic response of bending moment (unit: N·m)

$$M = \mu\varepsilon \cdot W \cdot E \cdot 10^{-9} \ (N \cdot m) \quad (1)$$

where με is the micro-strain, W is the section modulus in bending per unit length, and E is the elastic modulus of concrete. Fig. 14 shows the bending moment in the middle section and end section of the utility tunnel under the EL-Centro and Taft waves. In general, the bending moment at the corner point was much larger than that at the middle point, which was similar to the distribution of strain.

Table 8 Calculation parameters of the bending moment

Section height h/mm	Section width d/mm	Section modulus in bending W/mm3	Elasticity modulus E/MPa
20	1000	66666.67	6062.22

Comparatively, a similar result was reported by Abuhajar *et al*. (2015a). Moreover, the bending moment of the sidewalls at the bottom corner was larger than that at the top corner. For the top slab, the bending moment at the right corner was generally larger than that at the left corner, whereas for the bottom slab, the left corner exhibited a larger bending moment. This figure also indicates that the bending moment (neglecting the middle point) is amplified with increasing PGA under both EL-Centro and Taft waves. Furthermore, even with the same PGA, the bending moment response under the EL-Centro wave was more significant than that under the Taft wave, indicating that the bending moment of the utility tunnel was related not only to the input acceleration but also to the seismic wave types.

The bending moment of the two sidewalls in the end section was much larger than that in the middle section. In contrast, the top slab in the middle section exhibited a more significant response in the bending moment than that in the end section. For the bottom slab, the bending moment at the left corner of the end section was larger than that of the middle section, whereas at the right corner, the result was the opposite.

Under the action of seismic waves, the utility tunnel was pushed by the soil to swing left and right. Based on the bending moment in Fig. 14, it could be predicted that the deformation of the utility tunnel was similar to shear deformation under the action of an earthquake. However, the shear directions of the top and bottom slabs were opposite in view of the direction of the bending moment. Due to the shear action of the surrounding soil, the bending moment distribution along the cross-section exhibited a rotational trend.

4. Conclusions

In this study, a series of shaking table tests were carried out to investigate the seismic responses of a utility tunnel model under the EL-Centro and Taft waves. The salient conclusions from this study are as follows:

• The predominant frequency of the earthquake waves changed significantly along the soil depth, indicating the filtering effect on the low-frequency components and the amplification effects on the high-frequency components. However, for different types of earthquake waves, the predominant frequencies had negligible differences at the same depth. The amplitude of soil acceleration along the depth showed an obvious development of soil nonlinearity as the PGA increased, which was the same for uniform and non-uniform excitations, regardless of the types of earthquake waves or the types of tunnels (utility tunnel, traffic tunnel, immersed tunnel and deep buried pipeline).

• Under uniform excitation in the transverse direction, the accelerations of the structure and soil were generally similar to each other. The difference in structure and soil acceleration near the lower ends of the structure indicated that the separation of soil and the structure possibly occurred in this part as PGA increased. The acceleration response of the two sidewalls had good consistency. However, the predominant frequency and peak acceleration on the top slab were generally larger than those on the bottom slab.

• The peak horizontal soil pressure was larger near the top and bottom structure slabs and smaller in the middle, in which the pressure had an approximately "W"-shaped distribution along the soil depth. The larger horizontal soil pressure on the top and bottom edges of the structure indicated a rotational trend of the structure. When the PGA was larger than 0.8 g, the movement states of the soil surrounding the structure were disturbed, inducing a decrease in soil pressure. Vertical soil pressure was also observed during transverse vibration; however, the vertical soil pressure was generally smaller than the horizontal soil pressure.

• The seismic strains at the two corner points of the structure were slightly different, and the values were much larger at these points than at the middle point. Generally, the maximum strain of the cross-section in the end section was larger than that in the middle section, and the strain response on the outer surface was more significant than that on the inner surface.

• The middle point was not the most dangerous position. The bending moment at the corner points was the largest, which increased as the input acceleration increased. In addition, the seismic wave types had significant influences on the bending moment of the utility tunnel. The deformation of the utility tunnel under the action of an earthquake was similar to shear deformation. Due to the opposite shear directions of the top and bottom slabs produced by the surrounding soil, the cross-section exhibited a rotational trend.

Acknowledgments

The authors would like to acknowledge the funding from the National Natural Science Foundation of China (grant no. 51622803, 41831282), graduate research and innovation foundation of Chongqing, China (grant no. CYS18021).

References

Abuhajar, O., El Naggar, H. and Newson, T. (2015a), "Seismic soil-culvert interaction", *Can. Geotech. J.*, **52**(11), 1649-1667. https://doi.org/10.1139/cgj-2014-0494.

Abuhajar, O., El Naggar, H. and Newson, T. (2015b), "Experimental and numerical investigations of the effect of buried box culverts on earthquake excitation", *Soil Dyn. Earthq. Eng.*, **79**, 130-148. https://doi.org/10.1016/j.soildyn.2015.07.015.

Baziar, M.H., Moghadam, M.R., Kim, D.S. and Choo, Y.W. (2014), "Effect of underground tunnel on the ground surface acceleration", *Tunn. Undergr. Sp. Tech.*, **44**, 10-22. https://doi.org/10.1016/j.tust.2014.07.004.

Chen, H.J., Li, X.J., Yan, W.M., Chen, S.C. and Zhang, X.M. (2017), "Shaking table test of immersed tunnel considering the geological condition", *Eng. Geol.*, **227**, 93-107. https://doi.org/10.1016/j.enggeo.2017.05.014.

Chen, J., Jiang, L.Z., Li, J. and Shi, X.J. (2012), "Numerical simulation of shaking table test on utility tunnel under non-uniform earthquake excitation", *Tunn. Undergr. Sp. Tech.*, **30**, 205-216. https://doi.org/10.1016/j.tust.202012.02.023.

Chen, J., Shi, X.J. and Li, J. (2010), "Shaking table test of utility tunnel under non-uniform earthquake wave excitation", *Soil Dyn. Earthq. Eng.*, **30**(11), 1400-1416. https://doi.org/10.1016/j.soildyn.2010.06.014.

Chou, J.C., Kutter, B.L., Travasarou, T. and Chacko, J.M. (2010), "Centrifuge modeling of seismically induced uplift for the BART Transbay tube", *J. Geotech. Geoenviron. Eng.*, **137**(8), 754-765. https://doi.org/10.1061/(ASCE)GT.1943-5606.0000489.

Cilingir, U. and Madabhushi, S.P.G. (2011), "Effect of depth on the seismic response of square tunnels", *Soils Found.*, **51**(3), 449-457. https://doi.org/10.3208/sandf.51.449.

Debiasi, E., Gajo, A. and Zonta, D. (2013), "On the seismic response of shallow-buried rectangular structures", *Tunn. Undergr. Sp. Tech.*, **38**, 99-113. https://doi.org/10.1016/j.tust.2013.04.011.

Ding, X.M., Li, F., Wang, C.L., Chen, Z.X. and Han, L. (2020), "Shaking table tests of the seismic response of a utility tunnel with a joint connection", *Soil Dyn. Earthq. Eng.*, **133**, 106133. https://doi.org/10.1016/j.soildyn.2020.106133.

Fan, Z.F., Zhang, J.C., Xu, H. and Cai, J.H. (2019), "Transmission of normal p-wave across a single joint based on g-λ model", *Shock Vib.*, 1-10. https://doi.org/10.1155/2019/8240586.

Hashash, Y.M.A., Hook, J.J., Schmidt, B. and Yao, I.C. (2001), "Seismic design and analysis of underground structures", *Tunn. Undergr. Sp. Tech.*, **16**(4), 247-293. https://doi.org/10.1016/S0886-7798(01)00051-7.

Jiang, L.Z., Chen, J. and Li, J. (2010), "Seismic response of underground utility tunnels: Shaking table testing and FEM analysis", *Earthq. Eng. Eng. Vib.*, **9**(4), 555-567. https://doi.org/10.1007/s11803-010-0037-x.

Kwak, C., Jang, D., You, K. and Park, I. (2018), "Dynamic response on tunnel with flexible segment", *Geomech. Eng.*, **15**(3), 833-839. https://doi.org/10.12989/gae.2018.15.3.833.

Li, R.S., Chen, L.W., Yuan, X.M. and Li, C.C. (2017), "Experimental study on influences of different loading frequencies on dynamic modulus and damping ratio", *Chin. J. Geotech. Eng.*, **39**(1), 72-80 (in Chinese). https://doi.org/10.11779/CJGE201701005.

Liu, N., Huang, Q.B., Fan, W., Ma, Y.J. and Peng, J.B. (2018), "Seismic responses of a metro tunnel in a ground fissure site," *Geomech. Eng.*, **15**(2), 775-781. https://doi.org/10.12989/gae.2018.15.2.775.

Liu, X.R., Li, D.L., Wang, J.B. and Wang, Z. (2015), "Surrounding rock pressure of shallow-buried bilateral bias tunnels under earthquake", *Geomech. Eng.*, **9**(4), 427-445. https://doi.org/ 10.12989/gae.2015.9.4.427.

Shi, X.J. (2008), "Shaking table tests of utility tunnel under non-uniform earthquake wave excitation", Ph.D. Dissertation, Tongji University, Shanghai, China.

Sun, Q.Q., Bo, J.S. and Dias, D. (2019), "Viscous damping effects on the seismic elastic response of tunnels in three sites", *Geomech. Eng.*, **18**(6), 639-650. https://doi.org/10.12989/gae.2019.18.6.639.

Tsinidis, G. (2017), "Response characteristics of rectangular tunnels in soft soil subjected to transversal ground shaking", *Tunn. Undergr. Sp. Tech.*, **62**, 1-22. https://doi.org/10.1016/j.tust.2016.11.003.

Tsinidis, G., Pitilakis, K., Madabhushi, G. and Heron, C. (2015), "Dynamic response of flexible square tunnels: Centrifuge testing and validation of existing design methodologies", *Geotechnique*, **65**(5), 401-417. https://doi.org/10.1680/geot.SIP.15.P.004.

Tsinidis, G., Rovithis, E., Pitilakis, K. and Chazelas, J.L. (2016), "Seismic response of boxtype tunnels in soft soil: Experimental and numerical investigation", *Tunn. Undergr. Sp. Tech.*, **59**, 199-214. https://doi.org/10.1016/j.tust.2016.07.008.

Wang, G.B., Yuan, M.Z., Ma, X.F. and Wu, J. (2017), "Numerical study on the seismic response of the underground subway station-surrounding soil mass-ground adjacent building system", *Front. Struct. Civ. Eng.*, **11**(4), 424-435. https://doi.org/10.1007/s11709-016-0381-7.

Wang, Z.Z., Jiang, Y.J., Zhu, C.A. and Sun, T.C. (2015), "Shaking table tests of tunnel linings in progressive states of damage", *Tunn. Undergr. Sp. Tech.*, **50**, 109-117. https://doi.org/10.1016/j.tust.2015.07.004.

Xu, H., Li, T. B., Xia, L., Zhao, J.X. and Wang, D. (2016), "Shaking table tests on seismic measures of a model mountain tunnel", *Tunn. Undergr. Sp. Tech.*, **60**, 197-209. https://doi.org/10.1016/j.tust.2016.09.004.

Yan, K.M., Zhang, J.J., Wang, Z.J., Liao, W.M. and Wu, Z.J. (2018), "Seismic responses of deep buried pipeline under non-uniform excitations from large scale shaking table test", *Soil Dyn. Earthq. Eng.*, **113**, 180-192. https://doi.org/10.1016/j.soildyn.2018.05.036.

Yan, X., Yu, H. T., Yuan, Y. and Yuan, J.Y. (2015), "Multi-point shaking table test of the free field under non-uniform earthquake excitation", *Soils Found.*, **55**(5), 985-1000. https://doi.org/10.1016/j.sandf.2015.09.031.

Yu, H. T., Cai, C., Bobet, A., Zhao, X. and Yuan, Y. (2019), "Analytical solution for longitudinal bending stiffness of shield tunnels", *Tunn. Undergr. Sp. Tech.*, **83**, 27-34. https://doi.org/10.1016/j.tust.2018.09.011.

Yu, H.T., Yan, X., Bobet, A., Yuan, Y., Xu, G.P. and Su, Q.K. (2018c), "Multi-point shaking table test of a long tunnel subjected to non-uniform seismic loadings", *B. Earthq. Eng.*, **16**(2), 1041-1059. https://doi.org/10.1007/s10518-017-0223-6.

Yu, H.T., Yuan, Y., Qiao, Z.Z., Gu, Y., Yang, Z.H. and Li, X.D. (2013), "Seismic analysis of a long tunnel based on multi-scale method", *Eng. Struct.*, **49**, 572-587. https://doi.org/10.1016/j.engstruct.2012.12.021.

Yu, H.T., Yuan, Y., Xu, G.P., Su, Q.K., Yan, X. and Li, C. (2018b), "Multi-point shaking table test for long tunnels subjected to non-uniform seismic loadings - part II: Application to the HZM immersed tunnel", *Soil Dyn. Earthq. Eng.*, **108**, 187-195. https://doi.org/10.1016/j.soildyn.2016.08.018.

Yu, H.T., Zhang, Z.W., Chen, J.T., Bobet, A., Zhao, M. and Yuan, Y. (2018a), "Analytical solution for longitudinal seismic response of tunnel liners with sharp stiffness transition", *Tunn. Undergr. Sp. Tech.*, **77**,103-114. https://doi.org/10.1016/j.tust.2018.04.001.

Yuan, Y., Yu, H.T., Li, C., Yan, X. and Yuan, J.Y. (2018), "Multi-point shaking table test for long tunnels subjected to non-uniform seismic loadings – Part I: Theory and validation", *Soil Dyn. Earthq. Eng.*, **108**, 177-186. https://doi.org/10.1016/j.soildyn.2016.08.017.

Zhang, J.H., Yuan, Y. and Yu, H.T. (2019), "Shaking table tests on discrepant responses of shaft-tunnel junction in soft soil under transverse excitations", *Soil Dyn. Earthq. Eng.*, **120**, 345-359. https://doi.org/10.1016/j.soildyn.2019.02.013.

CC